Coherent isotropic averaging in zero-field nuclear magnetic resonance. II. Cubic sequences and time-reversal of spin couplings

A. Llor,[a] Z. Olejniczak,[b] and A. Pines
Materials Sciences Division, Lawrence Berkeley Laboratory, and Department of Chemistry, University of California, Berkeley, California 94720

(Received 23 January 1995; accepted 25 May 1995)

We present a special case of the theory of coherent isotropic averaging in zero-field NMR, given in part I of this work. In a zero external field, combinations of the magnetic-field pulses restricted to $\pi/2$ rotations along the three coordinate axes can selectively average internal spin Hamiltonians while preserving the intrinsic invariance of the spectrum with respect to the sample orientation. Compared with the general case, the limits of the allowed scaling factors of first- and second-rank interactions are slightly reduced. For instance, time reversal is possible for second-rank tensors with a $-1/5$ scaling factor, instead of $-1/4$ in general. Finite pulse compensations are analyzed and experimental illustrations are given for two optimum time-reversal sequences. The cubic sequences, though less efficient than the icosahedral sequences, are technically more feasible and may be used in zero-field experiments such as decoupling (by rank or nuclear species), time reversal or multipolar experiments (the zero-field equivalent of multiple-quantum NMR). © *1995 American Institute of Physics.*

I. INTRODUCTION

One of the main causes for the broadening of the NMR transitions observed on powdered or amorphous solids is the anisotropy of the local interactions due to the truncation by usually much stronger Zeeman field.[1,2] The broadening limits the resolution and can be removed by various coherent averaging techniques[2,3] (as MAS,[4] WHH,[5] DAS,[6] DOR,[7] ...), or by observing the spin couplings in a zero external field.[8] In the zero-field NMR technique (ZF-NMR) there is no Zeeman field to truncate the local interactions so there is no privileged orientation of the crystallites of the sample with respect to the laboratory frame.

Coherent averaging techniques[2] in standard NMR spectroscopy (here called ''high-field'' NMR, or HF-NMR) have also made possible a wide range of Hamiltonian manipulations, and led to the development of new experiments such as time reversal[9–11] and multiple-quantum NMR.[12] Coherent averaging schemes in ZF-NMR have so far seldom been explored, and that was for the purpose of spin decoupling only.[13,14] Following a preliminary communication[15] we recently presented a first part of this work,[16] which was the general theory of coherent isotropic scaling in ZF-NMR. This theory may be used to design new investigation methods such as the ''multipolar ZF-NMR,'' a zero-field analog of multiple-quantum NMR in a high field.[17]

The general concept of isotropic coherent schemes[15,16] was introduced to preserve one of the fundamental properties of the spin Hamiltonian in ZF-NMR: The energy levels of the effective Hamiltonian should be independent of the crystallite orientation with respect to the laboratory frame. Although some privileged orientations may exist in the laboratory frame, along which magnetic field pulses are applied, for example, it is required that the coherent process as a whole preserves the isotropic behavior of the system. As shown in the first part of this work,[16] the manipulations allowed under this general constraint are scalings of the interactions. The accessible range of scaling factors, depending on the rank of the interactions, was deduced from group-theoretical arguments. In the homonuclear case, the ranges of scaling factors for first- and second-rank tensors were found to be limited from $-1/3$ to 1, and from $-1/4$ to 1, respectively. Various combinations of scaling factors can be realized for experiments such as rank-selective decoupling.

In that general theory, no constraints whatsoever were imposed on the magnetic-field trajectories. However, in order to obtain all the optimal scaling factors, the simplest sequences had to be of icosahedral symmetry[15,16] with the technical implementation of these sequences rather demanding. We have now investigated the allowed isotropic scaling schemes under the circumstances where the magnetic field pulses are constrained to some specific axes and angles, and specifically, in the more practical case of $\pi/2$ pulses along three orthogonal axes, X, Y, and Z in the laboratory frame.[13,14] This is important, since the simplest experimental setup to generate magnetic field pulses in any direction consists of three orthogonal coils. The aim of this work is thus to analyze the corresponding set of allowed scaling factors, both in the δ-pulse limit and for finite-length pulses. Two useful examples, the optimum time reversal for first- and second-rank interactions, are explicitly examined and corresponding experimental results are shown. Other cases of scaling can be derived from the principles established in these examples. All the experiments were carried out on a modified version of our zero-field spectrometer[18] where, as described in the first part of this work,[16] pulse precision and stability had to be carefully controlled. Indeed, zero-field sequences contain more pulses than their analogues in high-field, and must be recycled in order to reduce the effects of

[a]Present address: 5, rue Saint Denis, 92100 Boulogne, France.
[b]Present address: Radiospectroscopy Division, Institute of Nuclear Physics, Radzikowskiego 152, 31-342 Kraków, Poland.

 0021-9606/95/103(10)/3982/16/$6.00

eddy currents, finite pulse lengths, and higher-order corrections to the average Hamiltonian.

In the following we shall assume that the reader is familiar with the concepts introduced in the first part of this work,[16] but we briefly summarize the main results to be used. The experiment is performed in a zero field by applying a series of dc-magnetic-field pulses $\{P_i\}$, which modulate the full, untruncated spin Hamiltonian of the system. In the first-order average Hamiltonian theory,[2] the coherent averaging scheme is described by a trajectory of configurations $\{R_i\}$, defined in SO(3). The rotations R_i are deduced from the magnetic-field pulses P_i according to

$$R_i=(P_i\cdot P_{i-1}\cdot\ \cdots\ \cdot P_2\cdot P_1)^{-1}\quad\text{or}\quad P_i=R_i^{-1}\cdot R_{i-1}, \tag{1}$$

and can be defined by their total rotation angles ω_i, and their rotation axes $\mathbf{n}_i$. For interactions of rank l, the isotropic constraint on the averaging process is fulfilled if and only if

$$\langle\chi_\lambda^l(\omega_i)Y_{\lambda\mu}(\mathbf{n}_i)\rangle_i=0, \tag{2}$$

for any λ and μ, where $1\leqslant\lambda\leqslant 2l$ and $-\lambda\leqslant\mu\leqslant\lambda$. The $Y_{\lambda\mu}$ are the spherical harmonics, the χ_λ^l are the generalized characters of the Wigner matrices, and the $\langle\ \rangle_i$ brackets stand for the average over i. Then the scaling factor is given by

$$k_l=\langle\chi^l(\omega_i)\rangle/(2l+1), \tag{3}$$

where χ^l is the character of the lth-order Wigner matrix. An important feature of Eq. (3) is that the scaling factor is independent of the rotation axes trajectory $\{\mathbf{n}_i\}$, and involves $\{\omega_i\}$ only. For first- and second-rank tensors this yields

$$k_1=(2\langle\cos\ \omega_i\rangle+1)/3, \tag{4a}$$

$$k_2=(4\langle\cos^2\ \omega_i\rangle+2\langle\cos\ \omega_i\rangle-1)/5. \tag{4b}$$

Isotropic sequences in which ω takes only one value (spherical sequences) can be generated using an icosahedral distribution of $\{\mathbf{n}_i\}$. Then, by combining spherical sequences of different ω values, the set of all the allowed scaling factors can be constructed.

II. CUBIC δ-PULSE SEQUENCES

In the previous problem of general isotropic scaling[16] it was necessary to examine so-called spherical sequences that involve only one value of ω (which can take any value between 0 and π). Then the analysis of the allowed scaling factors for arbitrary isotropic trajectories $\{R_i\}$ was carried out on the equivalent schemes that were obtained as combinations of spherical sequences characterized by the same distributions of ω values and weights $\{\omega_i\}$. Now we are going to apply the same approach to our present problem, which is the case of sequences involving $\pi/2$ pulses along the three coordinate axes. This restricts the set of accessible configurations to the cubic subgroup of SO(3), so a trajectory will be a subset $\{R_i\}$ of the 24 elements of the cubic group. Here, there are only four discrete values of ω allowed, at 0, $\pi/2$, $2\pi/3$ and π, with 1, 6, 8, and 9 elements, respectively. Except for the special case of $\omega=0$, sequences involving just one of these sets only will not be isotropic, although overall isotropic behavior may be achieved by combining the configurations from different sets.

To analyze the accessible range of scaling factors, it is convenient to introduce the highest symmetry allowed for the system, namely the cubic symmetry. Let us assume that $\{R_i\}$ is an isotropic sequence involving some subset of the cubic group O and yielding some combination of scaling factors (k_1,k_2). Then the symmetrized version given by $\{g\cdot R_i\cdot g^{-1}\}$, where g spans the entire O group, will also give the same scaling factors, because the distribution $\{\omega_i\}$ is unchanged. We thus obtain all the possible allowed scaling factors by *combining complete classes of cubic configurations* to build sequences. Such sequences, which are invariant under group O, will therefore be termed cubic.

The analysis of the isotropy constraint for cubic sequences based on the general formalism as given by Eq. (2) is not very convenient. Instead of the spherical irreducible tensor basis, we shall use the Cartesian tensors, which are more appropriate for cubic symmetry and have already been introduced in previous analyses of zero-field decoupling sequences.[13] The Hamiltonian is expanded in terms of the three spin operators I_X^u, I_Y^u, and I_Z^u for each nucleus u, where the directions X, Y, and Z are the three fixed laboratory axes. In the presence of residual fields (first-rank interactions) and spin–spin dipolar couplings (second-rank), the Hamiltonian becomes

$$H=\sum_{\alpha,u}A_\alpha^uI_\alpha^u+\sum_{\alpha\beta,u<v}B_{\alpha\beta}^{uv}I_\alpha^uI_\beta^v, \tag{5}$$

where α and β stand for X, Y, and Z, and the coefficients A_α^u and $B_{\alpha\beta}^{uv}$ depend on the strengths of the interactions and the orientations of the principal axes in the laboratory frame. Since the dipolar coupling is a second-rank tensor, $B_{\alpha\beta}^{uv}$ is symmetrical and traceless with respect to $\alpha\beta$.[13] Thus the bilinear terms can be expanded over the following second-rank Cartesian tensors:

$$\alpha\alpha=I_\alpha^uI_\alpha^v-\mathbf{I}^u\mathbf{I}^v/3, \tag{6a}$$

$$\alpha\beta=I_\alpha^uI_\beta^v+I_\beta^uI_\alpha^v. \tag{6b}$$

Since $XX+YY+ZZ=0$, the three $\alpha\alpha$ tensors are not independent and the six $\alpha\alpha$ and $\alpha\beta$ tensors do span a five dimensional space, as expected for a second-rank representation. We use the shorthand notation α to denote I_α^u. This notation displays some ambiguity since the symbols X, Y, and Z represent both the coordinate axes and the first-rank tensors but context should make the distinction clear. In this description the effects of rotations belonging to the cubic group are conveniently described by permutations within each of the α, $\alpha\alpha$, and $\alpha\beta$ sets. In other words, this is a decomposition of the first- and second-rank tensors into irreducible representations of the cubic group. A table of all the transformations has already been published:[13] The first-rank tensors behave

TABLE I. Scaling factors of the various terms of spin interactions averaged over cubic-group classes. The classes are labeled by the total angle rotation ω and contain n elements (the two classes at $\omega=\pi$ are distinguished as π and π'). First-rank interactions (associated with the irreducible representation F_1) are always isotropically scaled by factor k_1. Second-rank interactions can be decomposed over the $\alpha\alpha$ and $\alpha\beta$ type tensors (irreducible representations E and F_2), respectively scaled by $k_{\alpha\alpha}$ and $k_{\alpha\beta}$. The δ describes the isotropy imbalance with respect to k_2, the isotropic contribution of the classes to the second-rank scaling factor.

ω	n	k_1	$k_{\alpha\alpha}$	$k_{\alpha\beta}$	k_2	δ
0	1	1	1	1	1	0
$\pi/2$	6	1/3	0	$-1/3$	$-1/5$	$+1/5$
$2\pi/3$	8	0	$-1/2$	0	$-1/5$	$-3/10$
π	3	$-1/3$	1	$-1/3$	1/5	$+4/5$
π'	6	$-1/3$	0	1/3	1/5	$-1/5$

as an F_1 representation, and the second-rank tensors are decomposed into E and F_2 representations for $\alpha\alpha$ and $\alpha\beta$, respectively.[19]

The analysis of an arbitrary cubic sequence is now simplified: The effect of a pulse on the Hamiltonian is given by a linear transformation which is a cubic representation $D(R_i)$, and the first-order averaging is performed over the complete classes defined by the ω_i. In the following derivation, we shall use notation $R_{\omega i}$, where ω labels the class of the configuration, whereas index i is now restricted to label R_ω inside class ω. The first-order average Hamiltonian can then be written

$$\langle H\rangle=\sum_{\alpha,u} A^u_\alpha\langle D(R_{\omega i})I^u_\alpha\rangle+\sum_{\alpha\beta,u<v} B^{uv}_{\alpha\beta}\langle D(R_{\omega i})I^u_\alpha I^v_\beta\rangle, \tag{7}$$

and for each irreducible representation, for instance the $\alpha\alpha$, this yields

$$\begin{aligned}\langle D(R_{\omega i})\alpha\alpha\rangle_{i\omega}&=\langle D(R_{\omega i})\rangle_{\omega i}\alpha\alpha=\langle\langle D(R_{\omega i})\rangle_i\rangle_\omega\alpha\alpha\\&=\langle k_{\alpha\alpha}(\omega)Id\rangle_\omega\alpha\alpha=\langle k_{\alpha\alpha}(\omega)\rangle_\omega\alpha\alpha,\end{aligned} \tag{8}$$

where Id is the identity matrix. The fact that class averages induce scalings of each of the α's, $\alpha\alpha$'s, or $\alpha\beta$'s is a consequence of Schur's Lemma[19] [indeed $\langle D(R_{\omega i})\rangle_i$ commutes with any $D(R)$ in the group]. In consequence, because of different scaling factors for the two $\alpha\alpha$ and $\alpha\beta$ representations, the second-rank tensors are not isotropically scaled, whereas the first-rank ones always are. We recall that under icosahedral symmetry the scaling for both first- and second-rank tensors was always isotropic.[16] For each of the five cubic classes Table I summarizes the various scaling factors, which can be computed explicitly from the table of cartesian tensor transformations[13] or from the character table of the cubic group.[19]

The scaling differences between the $\alpha\alpha$ and $\alpha\beta$ representations account for the anisotropy of cubic sequences for second-rank tensors. The general theory of isotropic scaling provides a useful guide for combining different classes in an isotropic manner. The contribution of each ω value to the isotropic scaling k_2 is actually given by Eq. (4b), so the difference between the $\alpha\alpha$ or $\alpha\beta$ scalings with respect to k_2 provides the *isotropy imbalance* that has to be compensated. The isotropy imbalance, defined as

$$\delta=k_{\alpha\alpha}-k_2 \tag{9}$$

is given in Table I, together with k_1, $k_{\alpha\alpha}$, and $k_{\alpha\beta}$. To generate an isotropic cubic sequence, it will thus be necessary to combine different classes, or ω values, in such a way that

$$\langle\delta(\omega)\rangle_\omega=0. \tag{10}$$

Once the condition (10) is fulfilled, the difference $k_{\alpha\beta}-k_2$ is automatically compensated; it is always proportional to δ and of the opposite sign, since the isotropic scaling factor is given by the trace of D: $k_2=(2k_{\alpha\alpha}+3k_{\alpha\beta})/5$.

TABLE II. Scaling factors of four nontrivial, cubic, isotropic sequences that explore only two cubic classes. The combination of the classes defined by ω_1 and ω_2 with weights λ_1 and λ_2 give isotropic scalings of first and second-rank interactions given by k_1 and k_2, respectively. The points representing the sequences in the k_1,k_2 plane are shown in Fig. 1. The N is the total number of explored configurations in the sequences.

ω_1	λ_1	ω_2	λ_2	N	k_1	k_2	Point (Fig. 1)
$\pi/2$	3/5	$2\pi/3$	2/5	14	1/5	$-1/5$	D
$2\pi/3$	8/11	π	3/11	11	$-1/11$	$-1/11$	E
π	1/5	π'	4/5	9	$-1/3$	1/5	C
$\pi/2$	1/2	π'	1/2	12	0	0	F

Starting with one class ω, the simplest way to compensate for the imbalance $\delta(\omega)$ is to add another class whose imbalance has an opposite sign. The weights associated with such combinations may not be equal, but since they are always positive, the combined classes should have opposite signs of δ. Inspecting Table I, we find four possible combinations only (excluding the trivial identity class), which are listed in Table II. Except for the full decoupling sequence which combines the $\pi/2$ and π' classes, these sequences are optimal, since each displays the smallest span of ω and is thus the closest to the general theoretical limits.[16] Any other isotropic cubic sequence will be built from a combination of such sequences, so the allowed scaling factor combinations are obtained as the convex envelope of the discrete optimum values in the (k_1,k_2) plane. This is illustrated by the shaded area in Fig. 1. The reduction of the accessible scaling factors due to the cubic constraint is not excessive compared to the limits of general isotropic schemes.[16] In the important cases of rank-selective decoupling and time reversal, the restrictions with respect to the general case are as follows (see Fig. 1):

(1) Range of scaling factors for $l=1$ tensors while decoupling $l=2$ interactions: $k_1=-1/6$ to 1/3, instead of $-(\sqrt{5}-1)/6$ to $(\sqrt{5}+1)/6$;
(2) Range of scaling factors for $l=2$ tensors while decoupling $l=1$ interactions: $k_2=-1/8$ to 2/5, instead of $-1/5$ to 2/5;
(3) No change at all for the optimum time reversal of $l=1$ tensors, with $k_1=-1/3$, and $k_2=1/5$;
(4) Optimum time reversal of $l=2$ tensors with $k_2=-1/5$, instead of $-1/4$ (while $k_1=1/5$, instead of 1/6);

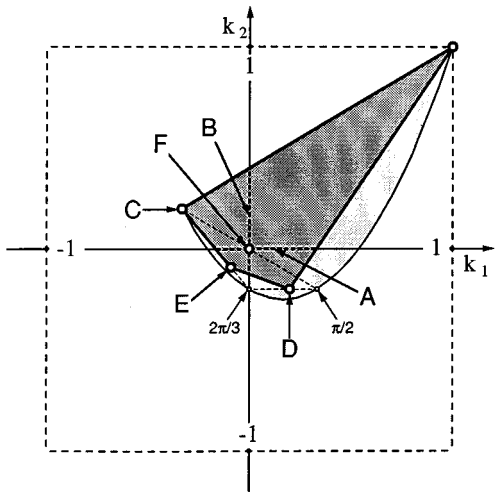

FIG. 1. Allowed combinations of isotropic scaling factors for first- ($l=1$) and second- ($l=2$) rank interactions, k_1 and k_2, are restricted to the shaded region of the (k_1,k_2) plane for cubic δ-pulse sequences. Various useful combinations of scaling factors are allowed: (A) decoupling of $l=2$ interactions, with scaling of $l=1$ tensors by $-1/6$ to $1/3$; (B) decoupling of $l=1$ interactions, with scaling of $l=2$ tensors by $-1/8$ to $2/5$; (C) optimal time-reversal scaling for $l=1$ interactions with $k_1=-1/3$, and $k_2=1/5$; (D) optimal time-reversal scaling for $l=2$ interactions with $k_1=1/5$, and $k_2=-1/5$; (E) optimal time-reversal scaling for both $l=1$ and $l=2$ interactions with $k_1=k_2=-1/11$. (F) decoupling of both $l=1$ and $l=2$ interactions with $k_1=k_2=0$. The isotropic scaling combinations associated with the $\pi/2$ and $2\pi/3$ configurations that belong to the cubic group are also shown. For comparison, the set of allowed combinations for unconstrained isotropic schemes is shown in light grey. As explained in Sec. II and listed in Table II, the D, E, and F points are obtained as the weighed averages of the $\pi/2$ and $2\pi/3$, the $2\pi/3$ and π, and the $\pi/2$ and π' configurations, respectively.

(5) Time-reversal scaling for both $l=1$ and 2 tensors with $k_1=k_2=-1/11$, instead of $-1/9$.

Explicit cubic sequences can be obtained after choosing a path to explore the various configurations. For the δ-pulse sequences, the order is usually irrelevant and since all the configurations are connected by a network of $\pi/2$ pulses, there is a wide range of possibilities. Some examples for decoupling and time reversal were previously given.[15] In practical situations, where the finite pulse lengths have to be taken into account, the path has to be chosen more carefully. We present some explicit pulse sequences in the discussion of experimental examples in Secs. IV and V.

Within the framework of orthogonal $\pi/2$ pulses only, one may wonder if the constraint of cubic symmetry of the trajectory is mandatory, i.e., if the configurations have to be explored by whole cubic classes. If not, simpler sequences could be obtained using, for instance, subgroups of the cubic group. Of course, the symmetry arguments presented above would not allow any improvement of the performance of the sequences as far as scaling factors are concerned, but shorter sequences could be expected. However, with smaller symmetry groups the number of irreducible representations in the subspace of second-rank tensors increases. It follows from the general principle of anisotropy compensation by combination of classes that more than two values of ω would be necessary in order to fulfill the isotropic condition. For instance, while using the tetrahedral group, we deal with three

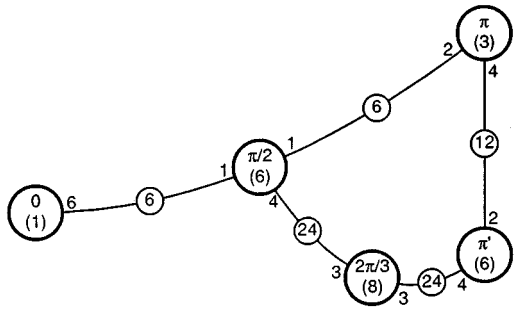

FIG. 2. Schematic network characteristics of the 24 configurations of the cubic group (regrouped into five cubic classes) with the $\pi/2$ pulses connecting them. Large circles stand for the cubic configurations (with their number in parentheses), while small circles indicate the number of $\pi/2$ paths connecting two classes. The number of paths per configuration is also shown by the class circles. This diagram allows us to design effective trajectories exploring the desired configurations and/or paths according to the cubic symmetry.

irreducible representations in the space of second-rank tensors (E_+, E_-, and F) and, accordingly, with three different partial scaling factors yielding two independent imbalance parameters. In general, three configurations are then needed to restore the isotropy and, as expected, the optimum sequences are eventually found to coincide with the cubic schemes explored above.

III. FINITE PULSE COMPENSATION OF CUBIC SEQUENCES

As discussed in part I,[16] the pulse compensation of isotropic schemes refers to the elimination of any anisotropic effects that might be introduced by the finite length of the pulses. Compared with the δ-pulse limit, the scaling factors may be somewhat affected by the compensation for the finite pulse lengths, but the isotropic behavior has to be preserved.

As already illustrated,[16] a continuous line of configurations inside SO(3) is explored during a pulse of finite length, and the average of the Hamiltonian over this path has to be included into the global average, as in Eqs. (2) and (3). Now, if a δ-pulse sequence exhibits a cubic symmetry, i.e. if the discrete set of explored configurations is a union of complete cubic classes, the version obtained by introducing $\pi/2$ pulses of finite length may no longer exhibit this symmetry. For the cubic symmetry to be fulfilled, the set of configurations in SO(3) has to be invariant under any cubic rotation g

$$\{R_i\}\rightarrow\{g\cdot R_i\cdot g^{-1}\}. \tag{11}$$

This means that if any $\pi/2$ path between two cubic configurations is used in a sequence, then all the other $\pi/2$ paths connecting the classes of those configurations have to be used as well, the same number of times with the same motion profile (i.e., the same pulse shapes have to be used in the three X, Y, and Z coils). For instance, the optimum time-reversal sequence for second-rank tensors (yielding a $-1/5$ scaling, see Table II) can be obtained by combining the six $\pi/2$ and eight $2\pi/3$ configurations into a 14-pulse sequence. Now, as shown in Fig. 2, the $\pi/2$ and $2\pi/3$ classes are con-

nected by 24 different $\pi/2$ paths, corresponding to the maximum number of elements under cubic symmetry. A cubic symmetric path in this case would thus require at least 24 pulses (this case is explored more extensively in Sec. V).

In general the shape of a real magnetic-field pulse is not rectangular, so the motion profile along the pulse path may not be linear (nonsquare shape pulse), affecting the corresponding average. Instead of assuming a specific pulse shape, we derive the compensation equations and the allowed scaling factors for the general case. Within this framework, deliberately modulated pulses are also allowed, which yields wider ranges of scaling factors. Instead of using the $\pi/2$ pulses, a sequence consisting of split pulses (for instance two $\pi/4$ pulses) could be implemented, while still keeping the configuration trajectory on the network of cubic $\pi/2$ paths. The set of allowed configurations is therefore extended from the four discrete ω values of the cubic group, to a continuous range of ω along the $\pi/2$ paths. The network of configurations is summarized in Fig. 2.

Depending on the choice of a particular pulse, a given configuration along this path will be symmetrized by the cubic group into 6, 12 or 24 other configurations. As in Eq. (8), the averaging is performed in two steps, first over the cubic group transformations (equivalent to the class average) and next over the configuration types. Let $M(R)$ be the transformation matrix, in the Cartesian tensor basis, associated with a given configuration R along a path. The transformation corresponding to the cubic average is given by

$$\begin{aligned}\langle M(R)\rangle_O &= \langle M(g\cdot R\cdot g^{-1})\rangle_{g\in O}\\ &= \langle D(g)\cdot M(R)\cdot D^{\dagger}(g)\rangle_{g\in O},\end{aligned} \tag{12}$$

where $D(g)$ is the representation of the cubic group in the space of first- or second-rank tensors. The adjoint transformation, as given in Eq. (11), acts on any matrix N according to

$$N\rightarrow \mathbf{S}_h(N)=D(h)\cdot N\cdot D^{\dagger}(h). \tag{13}$$

This is a representation of the cubic group in the space of linear transformations N, and since it leaves $\langle M(R)\rangle_O$ invariant, the $\langle M(R)\rangle_O$ belongs to the space of invariant irreducible representations. We must stress at this point that, by expanding the free Hamiltonian H over an irreducible tensor basis, the $M(R)$ can be written as a Wigner matrix [which is an irreducible representation of SO(3)]; however, the transformations involved in Eq. (13) belong to the *cubic group O* and thus $M(R)$, even in the Wigner matrix form, will be decomposed into irreducible representations of O.

According to Eq. (13), the decomposition of $\mathbf{S}$ in irreducible representations is given by the coupling between the representations D and $D^{\dagger}$. By introducing the expansion of D into irreducible representations, we can decompose the coupled representation in the following way:

$$\begin{aligned}D(g)\cdot D^{\dagger}(g) &= \left\{\sum_r D^{(r)}\right\}\left\{\sum_s D^{(s)\dagger}\right\}\\ &= \sum_{rs} D^{(r)}\cdot D^{(s)\dagger} = \sum_{rst}(rst)D^{(t)},\end{aligned} \tag{14}$$

where (rst) are the Clebsch–Gordan coefficients[19] of the cubic group (which couple the irreducible representations of the cubic group). A well known property of the Clebsch–Gordan expansion is that the coupled $D^{(r)}\cdot D^{(s)\dagger}$ contains the invariant representation (once) only if $r=s$.[19] For instance, for first-rank tensors, there is only one F_1 cubic irreducible representation in D, and therefore only one invariant representation. Just as for discrete sequences, this shows that first-rank tensors are isotropically scaled by the cubic symmetry. In the space of second-rank tensors, the D's are expanded into E and F_2 representations and, because they are different, there will be only two invariant representations corresponding to the $E\cdot E$ and $F_2\cdot F_2$ couplings. Thus the average $\langle M(R)\rangle_o$ performs the scalings of the $\alpha\alpha$ and $\alpha\beta$ type tensors, but not necessarily with the same factors. For both first- and second-rank tensors the situation is similar to that with δ pulses and we shall characterize the anisotropic contribution of a given configuration by the same parameter δ defined by Eq. (9). This is due to the fact that all the irreducible representations in the spaces of first- and second-rank tensors appear only once at the most. We will not attempt to derive the corresponding arguments for higher-rank tensors.

The imbalance $\delta(R)$ for the various possible paths is obtained by taking the partial traces (the invariant representations) of the transformation matrix $M(R)$ over the subspaces $\alpha\alpha$ and $\alpha\beta$, as given in Appendix A. The results are summarized in Table III, and by the δ vs ω diagram in Fig. 3. As in the δ-pulse limit [Eq. (10)], isotropic schemes must explore configurations and paths in such a way that the average of $\delta(R)$ vanishes. If, as mentioned above, we use split $\pi/2$ pulses, the sequences where ω takes only one value, i.e., spherical trajectories, can be generated for all ω values above $\omega_0=\arccos[(\sqrt{10}-4)/6]\approx 98.03°$. Below that value, as shown in Fig. 3, all the configurations of cubic $\pi/2$ paths have positive isotropy imbalances, and to compensate for them, some configurations with ω above 98.03° have to be used. The set

TABLE III. Isotropy imbalance for second-rank tensors of the configurations belonging to various types of $\pi/2$ paths in the cubic group. To simplify the analytical expressions the $0\rightarrow\pi/2$ and $\pi/2\rightarrow\pi$, as well as the $\pi/2\rightarrow 2\pi/3$ and $2\pi/3\rightarrow\pi'$ pulses have been regrouped to form single π pulses. The configurations are designated by the total angle α along these paths and c stands for $\cos\alpha$ (see also Fig. 3).

Path	α	$\cos\omega$	k_1	k_2	δ
$0\rightarrow\pi$	α_Z	c	$(2c+1)/3$	$(4c^2+2c-1)/5$	$(c-1)^2/5$
$\pi/2\rightarrow\pi'$	$\pi/2_Z+\alpha_Y$	$(c-1)/2$	$c/3$	$(c^2-c-1)/5$	$(3c^2+2c-3)/10$
$\pi\rightarrow\pi'$	$\pi_Z+\alpha_Y$	-1	$-1/3$	$1/5$	$c^2-1/5$

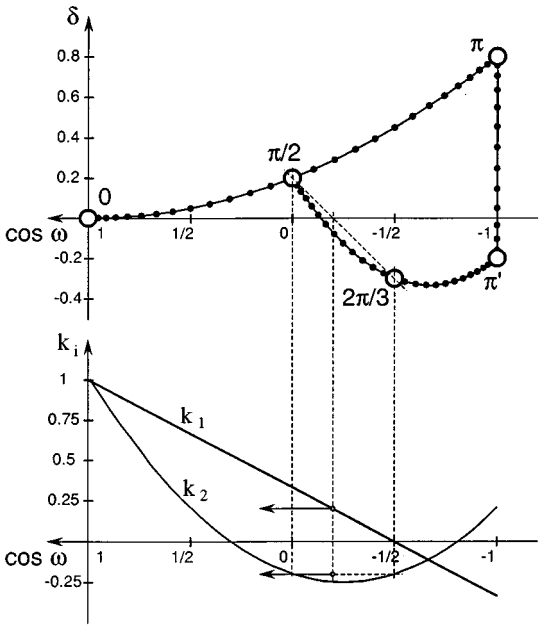

FIG. 3. Isotropy imbalance δ of second-rank interactions (defined in the text) for schemes containing $\pi/2$ pulses only along the fixed X, Y, and Z axes plotted as a function of cos ω, where ω is the total rotation angle of a configuration. By selecting a path which averages out δ we can generate an isotropic scaling sequence. The interval between successive black dots corresponds to 6° increases in the pulse angle between the cubic configurations indicated by the larger empty circles (see Sec. III). The corresponding plots of the first- and second-rank isotropic scaling factors k_1 and k_2 are also shown below. An example of second-rank isotropic sequence, combining the $2\pi/3$ and $\pi/2$ configurations, is shown by dashed lines.

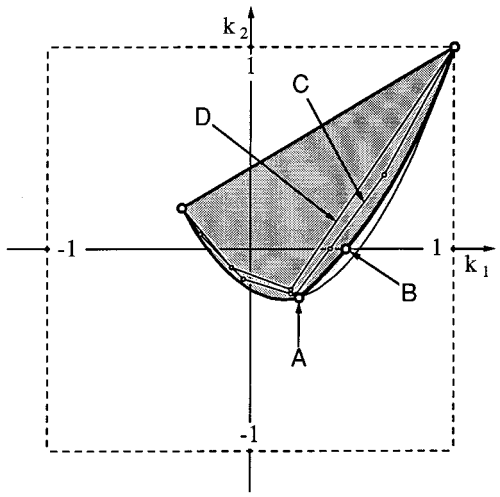

FIG. 4. Allowed combinations of isotropic scaling factors for first- ($l=1$) and second- ($l=2$) rank interactions, k_1 and k_2, are limited to the dark-shaded region of the (k_1,k_2) plane for sequences with pulses of unrestricted shape but of the axes along X, Y, or Z and of the total angle $\pi/2$ (cubic pulses). For comparison, the set of allowed combinations for completely unconstrained isotropic schemes is also shown in light grey. Spherical sequences (i.e., those that involve one value of ω only) cannot be generated for ω values below $\omega_0=\arccos[(\sqrt{10}-4)/6]$, corresponding to point A. This causes a reduction of about 13% in the first-rank scaling factor for the second-rank decoupling, as in point B at $(k_1,k_2)=(\sqrt{2}/3,0)$. With the supplementary constraint of rectangular shape for the $\pi/2$ pulses, the area of allowed scaling factors is further limited to the concave side of the polygonal line C (whose corner points are given in Table V). The limit for δ-pulse sequences D, already marked in Fig. 1, is also shown.

of allowed scaling factors in this region is determined in Appendix B and plotted in Fig. 4. Compared to the general isotropic limit defined by Eqs. (4), there is only a small reduction of the area of allowed scaling factor combinations: In the region of second-rank decoupling the maximum isotropic first-rank scaling is reduced by about 13%.

So far we have not introduced any constraint on the pulses. In real experiments, however, the local interactions are not negligible compared with the strengths of the available magnetic field pulses. The optimum pulse shape is rectangular in this case and, even if split pulses are used, the contribution of the pulses to the total isotropy imbalance and the scaling factors must be integrated over complete $\pi/2$ paths. The averages of δ, k_1, and k_2 over the five possible $\pi/2$ paths can be deduced from the expressions in Table III. They are listed in Table IV. The integrated pulse contributions can be considered as forming five discrete configurations that have to be combined with each other or with any cubic set of configurations in such a way that δ vanishes.

If we now exclude split pulses (so any single pulse is a complete $\pi/2$), then only the five original discrete cubic configurations can be combined with the five possible pulses. From this set of ten trajectory parts, five have positive, and four negative δ, giving a total of twenty possible isotropic combinations. The set of allowed scaling factors, shown in Fig. 4, will be given again by the convex envelope of the scaling-factor combinations. Table V lists the optimum schemes, i.e., schemes yielding scaling-factor combinations at the borderline of the allowed area. As expected, the area of allowed scaling factors in this case falls between the two limits found above for the δ pulses and for unrestricted cubic pulses.

The limit for rectangular pulses appears more realistic than that for the cubic pulses of unrestricted shape considered previously. As a matter of fact, the constraints imposed on the pulses are not sufficient, because, although the shape has to be rectangular, the relative amplitudes between different pulse sets have not been specified and the topological features of the network of $\pi/2$ paths have been overlooked. For instance, if all pulses have to be of the same amplitude, incommensurate weighing factors between different $\pi/2$ pulse sets (as in Table V) may be difficult to obtain in simple sequences. As shown in the examples of the next sections,

TABLE IV. Isotropy imbalance for second-rank tensors averaged over the various types of $\pi/2$ paths connecting the cubic configurations (square pulse shape is assumed). These values are obtained by integrating the expressions given in Table III over $\alpha=0$ to $\pi/2$ and $\alpha=\pi/2$ to π. The N is the number of different $\pi/2$ paths of a given type and has to be taken into account when combining the pulses and configurations to generate an isotropic sequence.

Path	N	k_1	k_2	δ
$0\rightarrow\pi/2$	6	$(\pi+4)/3\pi$	$(\pi+4)/5\pi$	$(3\pi-8)/10\pi$
$\pi/2\rightarrow\pi$	6	$(\pi-4)/3\pi$	$(\pi-4)/5\pi$	$(3\pi+8)/10\pi$
$\pi/2\rightarrow2\pi/3$	24	$2/3\pi$	$-(\pi+4)/10\pi$	$-(3\pi-8)/20\pi$
$2\pi/3\rightarrow\pi'$	24	$-2/3\pi$	$-(\pi-4)/10\pi$	$-(3\pi+8)/20\pi$
$\pi\rightarrow\pi'$	12	$-1/3$	1/5	3/10

TABLE V. Optimum isotropic cubic trajectories involving $\pi/2$ pulses of square shape. Starting from a given $\pi/2$ pulse-type the combinations with other pulses and cubic configurations are designed to average out the isotropy imbalance obtained from Tables I and III (see Figs. 2 and 3). Out of the twenty possible combinations excluding identity at $(k_1,k_2)=(0,0)$, only eight are optimal (i.e., they belong to the convex envelope of scaling factor combinations as shown in Fig. 4). Out of those eight, the one which combines discrete cubic configurations at π and $2\pi/3$ has already been listed in Table II. For the seven others a set of $\pi/2$ pulses is combined with discrete cubic configurations (five cases) or other $\pi/2$ paths (two cases) as listed in the table. The weighing factors are associated with the whole sets of either pulses or configurations, and effective sequences have thus to take into account the number of elements in each set (given by N in Tables I and III).

Config./Path	Weight	Config./Path	Weight	k_1	k_2
$0\rightarrow\pi/2$	$\frac{3\pi}{6\pi-8}$	$2\pi/3$	$\frac{3\pi-8}{6\pi-8}$	$\frac{\pi+4}{6\pi-8}$	$\frac{2}{3\pi-4}$
$0\rightarrow\pi/2$	$\frac{1}{3}$	$\pi/2\rightarrow 2\pi/3$	$\frac{2}{3}$	$\frac{\pi+8}{9\pi}$	0
$\pi/2$	$\frac{3\pi-8}{7\pi-8}$	$\pi/2\rightarrow 2\pi/3$	$\frac{4\pi}{7\pi-8}$	$\frac{\pi}{7\pi-8}$	$-\frac{\pi}{7\pi-8}$
$\pi/2\rightarrow\pi$	$\frac{3\pi-8}{9\pi+8}$	$\pi/2\rightarrow 2\pi/3$	$\frac{6\pi+16}{9\pi+8}$	$\frac{3\pi^2-8\pi+64}{3\pi(9\pi+8)}$	$-\frac{8}{9\pi+8}$
$\pi/2\rightarrow\pi$	$\frac{3\pi}{6\pi+8}$	$2\pi/3$	$\frac{3\pi+8}{6\pi+8}$	$-\frac{-\pi+4}{6\pi+8}$	$-\frac{2}{3\pi+4}$
π	$\frac{3}{11}$	$2\pi/3$	$\frac{8}{11}$	$-\frac{1}{11}$	$-\frac{1}{11}$
π	$\frac{3\pi+8}{19\pi+8}$	$2\pi/3\rightarrow\pi'$	$\frac{16\pi}{19\pi+8}$	$-\frac{3\pi+40}{57\pi+2}$	$\frac{-\pi+8}{19\pi+8}$
$\pi\rightarrow\pi'$	$\frac{2}{5}$	π'	$\frac{3}{5}$	$-\frac{1}{3}$	$\frac{1}{5}$

each experimental case requires a specific analysis. However, the area of allowed scaling factor combinations that has been calculated above with the rectangular-pulse assumption gives a reasonable estimate for the performance of real sequences.

Although the natural symmetry to build isotropic schemes for second-rank tensors in SO(3) is icosahedral, it is interesting to note that the cubic symmetry can do almost equally well. The smaller areas of allowed scaling factors in Figs. 1 and 4 should not be seen as coming from the symmetry but from the stringent condition of orthogonal $\pi/2$ pulses in the sequences. This restricts the allowed configurations near the origin to *positive values of imbalance only*. They could be actually compensated by using configurations at the same ω values but with opposite imbalance, for instance along the magic directions. The symmetry of the arrangement would still be cubic and spherical sequences would then be available for any value of ω. In the formalism of irreducible tensors used in the first part of this work,[16] this means that the cubic symmetry can average out up to fourth-rank spherical harmonics. Although the general group-theoretical arguments show that one fourth-rank spherical harmonic is not averaged out by the cubic group,[20] there are specific point distributions of this symmetry that do average out this remaining term (and even remaining terms of higher ranks).[21] Such distributions are already well known for spherical quadratures,[21] but, for second-rank tensors, the cubic sequences will in terms of number of points always be less efficient than the corresponding icosahedral sequences. Examples are provided by the two naturally spherical cubic sets of configurations, found at $\omega_0=\arccos[(\sqrt{10}-4)/6]$ and at $\omega=\pi$ (see Fig. 3). They contain, respectively, 24 and 12 different configurations, compared to 12 and 6 for the icosahedral solutions.

IV. GENERATING REAL SEQUENCES: TIME REVERSAL FOR FIRST-RANK COUPLINGS

As in high-field NMR,[2] pulse sequences in zero field have to be compensated for various error sources: finite pulse lengths, effects of higher-order terms in the average Hamiltonian, as well as pulse errors and inhomogeneities. The finite width of the pulses is compensated using the general principles of the previous sections. The second-order corrections due to the finite duration of the sequence are eliminated by time-symmetrized sequences[2] and this also compensates for the residual rotation after one cycle due to the pulse errors (provided that opposite pulses are properly balanced, and even if they are inhomogeneous or poorly calibrated). However, pulse errors and inhomogeneities affect also the average Hamiltonian by generating configuration paths that do not follow the ideal trajectory. Although this last problem has been addressed in a high-field NMR,[2] we shall not attempt to devise the corresponding schemes in a zero field.

In all the sequences used in the experiments shown below, one cycle $\{R_i\}_{0\leqslant i\leqslant n}$ is compensated by the next cycle $\{R_{n-i}\}_{0\leqslant i\leqslant n}$, where the configurations are explored in the reverse order. It follows from Eq. (1) that the pulses in the symmetric cycle are opposite and applied in the reverse order compared to the pulses in $\{R_i\}_{0\leqslant i\leqslant n}$. In contrast with the high-field situation where opposite pulses are just related through a phase shift of π, opposite dc pulses are obtained by applying physically opposite currents in the pulse coils.

This has another significant advantage: the reduction of eddy currents effects. Ideally, the coils that generate the dc pulses in ZF-NMR should have no metallic parts in their vicinity to avoid the generation of eddy currents,[14,18] but few experimental setups can perfectly comply to this condition. Then, for a given pulse sequence, the time average of the magnetic-field pulses has to vanish in order to avoid the build up of steady residual magnetic fields from the eddy currents. This is automatically ensured by the symmetrization for the second-order compensation.

When using time-symmetrized cycles to compensate for the second-order effects, it is possible to get rid of two pulses between the two time-symmetric subcycles. This is extensively used in high-field sequences (such as WHH[2,5]) to reduce somewhat the average irradiation power and to eliminate any rotations around the magnetic-field axis Z (X and Y rotations are obtained with single rf pulses whereas Z rotations require composite transverse pulses, or dc pulses along Z). In contrast, the elimination of two pulses in zero-field sequences is not very useful: All the pulse directions are equivalent and, because of the higher number of pulses per cycle, the reduction of the average power is negligible. Furthermore, for symmetry arguments, the compensation for the finite length of the pulses is achieved more efficiently when preserving all the pulses of a subcycle. All the second-order compensated sequences will thus consist of complete subcycles containing their total number of pulses as given in the noncompensated versions.

Isotropic sequences for first-rank interactions were examined in the first part of this work.[16] If isotropy for second-rank tensors is not required, the general principles of isotropic scaling show that configuration distributions of tetrahedral symmetry are sufficient. Such schemes were already given for decoupling,[13,15] and for the δ-pulse versions of time reversal.[15,16] They are simple illustrations of the general cubic formalism introduced in the previous sections, since the tetrahedral group T is a subgroup of the cubic group O.

Optimum time reversal of $l=1$ tensors is obtained with configurations on the $\omega=\pi$ sphere of SO(3).[16] A tetrahedrally symmetric set of points necessarily contains 1, 4, 6, or 12 elements, so in general the minimum number of configurations for isotropic tetrahedral sequences is 4. However, as already pointed out,[16] the folded structure of SO(3) allows us to reduce these numbers in the case of the $\omega=\pi$ sphere. The simplest case, as shown in Fig. 5, consists of the three π configurations of the cubic group. In the δ-pulse limit the sequence contains three π pulses[15,16]

$$\pi_Z-(\tau/2-\pi_Y-\tau-\pi_Z-\tau-\pi_X-\tau/2)_n-\pi_Z. \tag{15}$$

where, as explained in the Appendix of the first part of this work,[16] the pulses have been computed according to Eq. (1), assuming that they correspond to *active, right-handed rotations of the spin magnetization*. We shall use this definition in all the sequences listed below. After symmetrization for second-order corrections, the three-pulse building block yields a six-pulse cycle with two sampling points

$$\pi_Z-(\tau/2-\pi_Y-\tau-\pi_Z-\tau-\pi_X-\tau-\pi_{-X}-\tau-\pi_{-Z}-\tau-\pi_{-Y}-\tau/2)_n-\pi_Z. \tag{16}$$

For pulses of finite length, the tetrahedral symmetrization of the trajectory yields six different π paths (see Fig. 5). Each vertex is connected to the others by an even number of π paths which makes it possible to explore all the paths just once with a six-pulse sequence. Starting from the simple three-pulse sequence (15), there are two possible ways of generating such a trajectory

$$\pi_Z-(\tau/2-\pi_Y-\tau-\pi_Z-\tau-\pi_X-\tau-\pi_X-\tau-\pi_Z-\tau-\pi_Y-\tau/2)_n-\pi_Z, \tag{17a}$$

$$\pi_Z-(\tau/2-\pi_Y-\tau-\pi_Z-\tau-\pi_X-\tau-\pi_{-Y}-\tau-\pi_{-Z}-\tau-\pi_{-X}-\tau/2)_n-\pi_Z. \tag{17b}$$

An interesting feature of the first version is that the π_Z, π_X, and π_Y configurations are explored in the reverse order in the second half of the cycle, so second-order effects are partly compensated (they are not for the pulses themselves). However, this is not achieved with the usual method of opposite pulses in reverse order, and thus eddy currents are not compensated. By contrast, in the second version, the eddy currents are compensated whereas the second-order effects are not.

Since none of the six-pulse sequences for time reversal allows us to compensate for all the major error sources simultaneously, some more complex versions had to be used in the experiments. As for high-field sequences,[2] they were generated with a building-block approach, where the most significant effects were treated first. In the present experiment

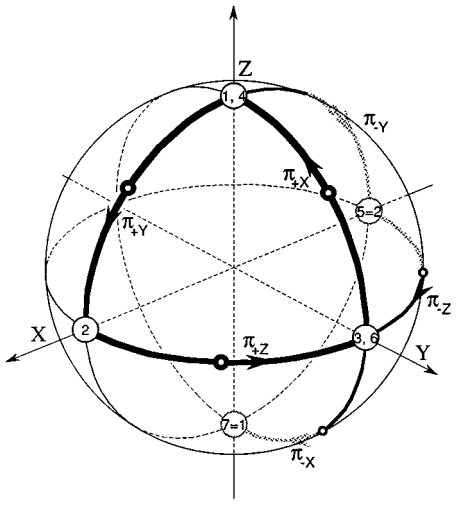

FIG. 5. Configuration trajectories in the SO(3) sphere for isotropic time reversal of first-rank interactions. In the δ-pulse version only the three π configurations of the cubic group are needed (points 1, 2, and 3, along the X, Y, and Z axes) and they are connected by three π pulses [sequence (15)]. This path (heavy line) can be compensated for the finite length of the pulses by adding three pulses to obtain a path of cubic symmetry, as shown by the medium heavy line [sequence (17b)]. Note that opposite configurations on the π sphere represent identical elements of SO(3), so the seemingly open path is actually closed. These trajectories can be made isotropic for the second-rank tensors as well by stopping at the π' configurations, as shown by empty dots along the π paths, according to the relative weights given in Tables II and V.

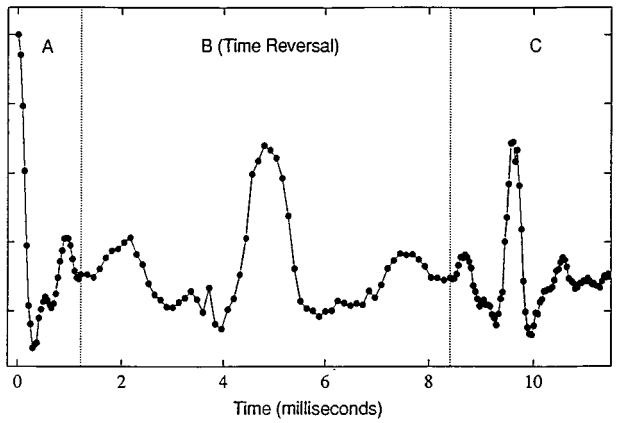

FIG. 6. Isotropic spin echoes for first-rank interactions: (A) The magnetization of the protons in a sample of water decays in the low residual magnetic field (which varies both in direction and in magnitude over the sample) in the zero-field NMR spectrometer; (B) The isotropic time-reversal sequence (5) is applied after 1.2 ms of free evolution, and generates an echo 3.6 ms later, because the scaling factor is $-1/3$; (C) Free evolution is resumed at 8.4 ms, resulting in a second echo at 9.6 ms. The 24-pulse sequence was compensated for the second-order effects and finite pulse lengths (see Sec. IV). The signal was sampled at every 3-pulse subcycle of 120 μs and the π-pulse duration was 2 μs.

the pulses were much stronger than the local interaction, so the first effects to be compensated for were a second-order term in the average Hamiltonian and eddy currents. Accordingly, we used the following 24-pulse sequence:

$$\begin{aligned}\pi_Z-(\tau/2-\pi_Y-\tau-\pi_Z-\tau-\pi_X-\tau-\pi_{-X}-\tau-\pi_{-Z}-\tau\\ -\pi_{-Y}-\tau-\pi_{-Y}-\tau-\pi_{-Z}-\tau-\pi_{-X}-\tau-\pi_X-\tau\\ -\pi_Z-\tau-\pi_Y-\tau-\pi_{-Y}-\tau-\pi_{-Z}-\tau-\pi_{-X}-\tau\\ -\pi_X-\tau-\pi_Z-\tau-\pi_Y-\tau-\pi_Y-\tau-\pi_Z-\tau-\pi_X-\tau\\ -\pi_{-X}-\tau-\pi_{-Z}-\tau-\pi_{-Y}-\tau/2)_n-\pi_Z,\end{aligned} \tag{18}$$

where the sampling periods appear every three pulses. The 6-pulse blocks compensate for the second-order effects and eddy currents, the 12-pulse subcycles include finite pulse-length corrections, and finally the 24-pulse total cycle cancels the second-order terms arising from the configurations explored during the pulses, which are not taken into account otherwise.

All these sequences are isotropic for first-rank tensors only. They can be made isotropic for second-rank interactions according to the general principles given in the previous sections. For the δ-pulse sequences, the isotropy imbalance of the π configurations has to be compensated by the π' configurations, as given in Table II. Since there are six π' configurations, they can be included in the trajectory of sequence (16) by replacing all the π pulses with successive $\pi/2$ pulses according to

$$\pi_i-\tau\rightarrow(\pi/2)_i-2\tau/3-(\pi/2)_i-\tau/3, \tag{19}$$

yielding 12-pulse sequences. As in Eq. (17b), this scheme reduces the influence of eddy currents and is also compensated for the effect on first-rank interactions of the finite length of the pulses. For second-rank tensors, the isotropic imbalance of the pulses has also to be corrected. According to Table V, the substitution (19) becomes

$$\pi_i-\tau\rightarrow(\pi/2)_i-(2\tau/3+3\tau')-(\pi/2)_i-\tau/3, \tag{20}$$

where τ' is the duration of the $\pi/2$ pulses.

The 24-pulse sequence (18) was tested on the proton NMR of a water sample in our zero-field spectrometer, where the zero-field shimming coils were deliberately set far from their optimal values. The residual field was a superposition of a constant 0.2×10^{-4} T along the Y direction, and of a gradient along Z, of 0.4×10^{-4} T over the sample height. In this way the residual field varied in both the magnitude (from about 0.2×10^{-4} T to 0.3×10^{-4} T) and the orientation (by about 90°) over the sample. In order to avoid the ''locking'' of the magnetization in the YZ plane initial and final pulses were added to follow the evolution by monitoring the polarization along X. The time-reversal effect was observed by generating an echo, as shown in Fig. 6. The decay of the signal was monitored under free evolution in the inhomoge-

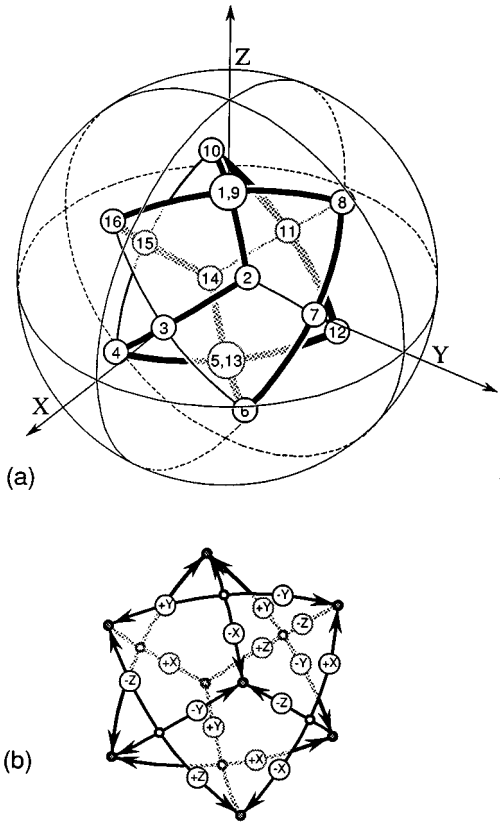

FIG. 7. Configuration trajectories in the SO(3) sphere for isotropic time reversal of second-rank interactions. In the δ-pulse version, as in sequence (21), 16 $\pi/2$-pulses are needed to explore 14 cubic configurations at $\omega=\pi/2$ and $2\pi/3$ [points labeled 1 to 16 along the path shown by the heavy line in (a)]. This path has a D_4 symmetry along the Z axis and, in order to compensate for the finite pulse lengths in a cubic-symmetric way, it is repeated after $2\pi/3$ rotations along the magic $\langle111\rangle$ direction, as in sequence (23). To facilitate the derivation of sequences (21) to (25), the pulses joining the vertices of the trajectory are shown in (b), as calculated from the $\pi/2$ to the $2\pi/3$ configurations according to Eq. (1).

neous field, up to a time t, when the sequence was applied, so at time $4t$ the echo was recovered from the depolarized sample, showing the time-reversal effect with a scaling factor equal to 1/3. A secondary echo was also obtained by further application of the sequence followed by a free evolution. The damping of the echoes is due to the inhomogeneities and errors in the pulses coming from eddy currents contributions and, in a smaller degree, to pulse imperfections.

V. TIME REVERSAL OF SECOND-RANK COUPLINGS

The previous section illustrated the methods to generate isotropic cubic sequences. This example was fairly simple: three configurations and an even number of paths connecting each of them to its neighbors. We shall now treat the case of time reversal for second-rank interactions. It is more complex but has also a broader range of applications, for instance, in the ''multipolar zero-field NMR'' experiments which are analogous to the multiple-quantum NMR techniques.

As listed in Table II, second-rank time reversal is achieved with a $-1/5$ scaling factor by combining the six and eight configurations at $\pi/2$ and $2\pi/3$, respectively. The configurations, together with the 24 $\pi/2$ paths that join them, are shown in Fig. 7 embedded in the SO(3) sphere representation. Although there is a total of 14 configurations, 16 pulses of $\pi/2$ are required to explore all of them: indeed, there are 8 configurations at $2\pi/3$ to be explored at least once, by following $\pi/2$ paths that never directly connect two such vertices. Since all the $\pi/2$ paths connect $2\pi/3$ to $\pi/2$ configurations, the $\pi/2$ vertices will be explored eight times also, although there are only six of them. Thus, in the simplest version of the cycle, there are two of the $\pi/2$ configurations that must be explored twice. These configurations can be chosen to be opposite in sign, as in Fig. 7, to preserve the highest symmetry possible. Many topologically different paths can now be used, but again, in order to achieve higher symmetry, we shall select a trajectory invariant under D_4 (a subgroup of the cubic group O).

At this point there are still two unequivalent ways of exploring the path of Fig. 7. In order to reduce the effect of eddy currents we shall retain the path involving an equal number of positive and negative pulses in each of the coils [this was not possible in one cycle for the first-rank time reversal in Eq. (15)]. In the δ-pulse limit, we can thus achieve the second-rank time reversal with the following sequence:

$$
\begin{aligned}
&(\pi/2)_{-Z}-(\tau/2-(\pi/2)_{-X}-\tau-(\pi/2)_{Y}-2\tau-(\pi/2)_{Y}-\tau\\
&\quad-(\pi/2)_{X}-\tau-(\pi/2)_{-Y}-\tau-(\pi/2)_{X}-2\tau-(\pi/2)_{X}-\tau\\
&\quad-(\pi/2)_{Y}-\tau-(\pi/2)_{X}-\tau-(\pi/2)_{-Y}-2\tau\\
&\quad-(\pi/2)_{-Y}-\tau-(\pi/2)_{-X}-\tau-(\pi/2)_{Y}-\tau\\
&\quad-(\pi/2)_{-X}-2\tau-(\pi/2)_{-X}-\tau-(\pi/2)_{-Y}-\tau/2)_{n}\\
&\quad-(\pi/2)_{Z},
\end{aligned}
\tag{21}
$$

where the time spent at the various configurations is weighed according to Table II. It is noticeable that, except for the initial and final $\pi/2$ pulses, this sequence contains pulses along X and Y only. It is an isotropic, zero-field analog, of the ''magic sandwich'' in a high field.[11]

At this stage it is desirable to compensate for the second-order contributions to the average Hamiltonian by time-symmetrization of the cycle in Eq. (21). Just as in HF-NMR sequences,[2] this is done prior to the compensation for the finite length of the pulses, because the cycle time has to be made as long as possible (but smaller than the characteristic time scale of the local interactions), in order to reduce the influence of pulse errors. Let us denote the main time period of the interaction, the subcycle duration, and the total duration of the pulses in the subcycle by T, T_C, and T_P, respectively, and let A be the average relative magnitude of the anisotropic contributions due to the finite length of the pulses. After one cycle, in the second order, the magnitudes of the different terms in the average interaction are

$$
1/(5T), \quad A(T_P/T_C)/T, \quad T_C/(2T^2), \tag{22}
$$

for the scaled interaction, the anisotropic scaled parts of the interaction, and the second-order average Hamiltonian, respectively. The ratio between the last two terms is thus $A(T/T_C)(T_P/T_C)$. Usually (T/T_C) is chosen around 5 to 10, while in practice (T_P/T_C) is always below 1 and seldom above 1/2. The ratio between the two leading corrections is thus determined by A, which, as will be shown below, can vary considerably, depending on the adjustments of the various time intervals. In more refined versions the A can be reduced from about 1/8 in Eq. (21) to as low as 1/100. We can thus say that the leading correction term is the second-order average Hamiltonian and that time symmetrization of the elementary cycle in Eq. (21) has to be carried out before any other compensation.

The last step consists in compensating for the finite length of the pulses in Eq. (21), or its second-order symmetrized version. There are 24 different $\pi/2$ paths connecting the $\pi/2$ and $2\pi/3$ configurations and, as shown in Fig. 7, each $2\pi/3$ vertex is connected by three such paths. As already mentioned in Sec. III, it is thus impossible to explore all of the 24 paths just once with a continuous trajectory. The compensation for the finite length of the pulses in this case involves necessarily a trajectory containing each $\pi/2$ path twice, yielding a 48-pulse sequence. Since the δ-pulse cycle (21) contains 16 pulses, it is natural to combine three such cycles. The trajectory in Fig. 7 is symmetrized by applying $2\pi/3$ rotations along the $\langle 111\rangle$ direction, but then the cycles have to start at a $2\pi/3$ configuration that is invariant under the C_3 rotations along $\langle 111\rangle$, for instance at the $2\pi/3_{\langle 111\rangle}$. According to the pulse definitions of Fig. 7, we thus find

$$(\pi/2)_{-Z}-(\pi/2)_{-X}-[(\tau/2-(\pi/2)_Y-(2\tau+k\tau')-(\pi/2)_Y-\tau-(\pi/2)_X-\tau-(\pi/2)_{-Y}-\tau-(\pi/2)_X-(2\tau+k\tau')$$
$$-(\pi/2)_X-\tau-(\pi/2)_Y-\tau-(\pi/2)_X-\tau-(\pi/2)_{-Y}-(2\tau+k\tau')-(\pi/2)_{-Y}-\tau-(\pi/2)_{-X}-\tau-(\pi/2)_Y-\tau$$
$$-(\pi/2)_{-X}-(2\tau+k\tau')-(\pi/2)_{-X}-\tau-(\pi/2)_{-Y}-\tau-(\pi/2)_{-X}-\tau/2)-(16\text{-pulse cycle with } X\rightarrow Y \text{ and } Y\rightarrow Z)$$
$$-(16\text{-pulse cycle with } X\rightarrow Z \text{ and } Y\rightarrow X)]_n-(\pi/2)_X-(\pi/2)_Z, \tag{23}$$

with three sampling points per cycle. Additional time delays at the $\pi/2$ configurations $k\tau'$ have been inserted to compensate for the isotropy imbalance introduced by the pulses of duration τ'. Using the result listed in Table V, one can find that $k=3-8/\pi\approx 0.454$, because $k\tau'$ is inserted at four out of six $\pi/2$ configurations. The time delays are inserted in the first cycle according to the D_4 symmetry (instead of the usual cubic symmetry) in order to compensate for the isotropy imbalances for each of the 16-pulse subcycles as much as possible. Indeed, Fig. 7 shows that the trajectory is more ''dense'' along the Z axis, and in order to improve the isotropy imbalance of one subcycle it is reasonable to add ''more'' configurations in the equatorial plane, although the $2\pi/3$ cycling along the $\langle 111\rangle$ axis eventually restores the full cubic symmetry in the global 48-pulse sequence (23). A rigorous proof of this intuitive point is given in Appendix C, together with the derivation of the least anisotropic version

$$(\pi/2)_{-Z}-(\pi/2)_{-X}-[((\tau/2+\kappa'\tau')-(\pi/2)_Y-(2\tau+k\tau')-(\pi/2)_Y-(\tau+k'\tau')-(\pi/2)_X-\tau-(\pi/2)_{-Y}-(\tau+k'\tau')$$
$$-(\pi/2)_X-(2\tau+k\tau')-(\pi/2)_X-(\tau+k'\tau')-(\pi/2)_Y-\tau-(\pi/2)_X-(\tau+k'\tau')-(\pi/2)_{-Y}-(2\tau+k\tau')-(\pi/2)_{-Y}$$
$$-(\tau+k'\tau')-(\pi/2)_{-X}-\tau-(\pi/2)_Y-(\tau+k'\tau')-(\pi/2)_{-X}-(2\tau+k\tau')-(\pi/2)_{-X}-(\tau+k'\tau')-(\pi/2)_{-Y}-\tau$$
$$-(\pi/2)_{-X}-\tau/2)-(16\text{-pulse cycle with } X\rightarrow Y \text{ and } Y\rightarrow Z)-(16\text{-pulse cycle with } X\rightarrow Z \text{ and } Y\rightarrow X)]_n$$
$$-(\pi/2)_X-(\pi/2)_Z, \tag{24}$$

where $k=1/\pi+3/4\approx 1.07$ and $k'=3/\pi-3/4\approx 0.205$. An average magnitude of the residual anisotropy in the D_4 symmetric subcycles can be determined: Considering the Hamiltonian partially averaged over the pulses (with their compensating time delays), the sequences (23) and (24), respectively, leave about 5% and 1% of the free interactions, compared to the 20% isotropic scaling factor. In situations where the pulse length is not negligible, sequence (24) is thus preferable. Both Eq. (23) and Eq. (24) are valid in the ''windowless'' limit, i.e., when $\tau=0$, and can be adapted with time-symmetrized subcycles to yield 96-pulse sequences as

$$(\pi/2)_{-Z}-(\pi/2)_{-X}-[((\tau/2+k'\tau')-(\pi/2)_Y-(2\tau+k\tau')-(\pi/2)_Y-(\tau+k'\tau')-(\pi/2)_X-\tau-(\pi/2)_{-Y}-(\tau+k'\tau')$$
$$-(\pi/2)_X-(2\tau+k\tau')-(\pi/2)_X-(\tau+k'\tau')-(\pi/2)_Y-\tau-(\pi/2)_X-(\tau+k'\tau')-(\pi/2)_{-Y}-(2\tau+k\tau')-(\pi/2)_{-Y}$$
$$-(\tau+k'\tau')-(\pi/2)_{-X}-\tau-(\pi/2)_Y-(\tau+k'\tau')-(\pi/2)_{-X}-(2\tau+k\tau')-(\pi/2)_{-X}-(\tau+k'\tau')-(\pi/2)_{-Y}-\tau$$
$$-(\pi/2)_{-X}-\tau/2)-(\text{time-symmetric 16-pulse cycle})-(16\text{-pulse cycle with } X\rightarrow Y \text{ and } Y\rightarrow Z)$$
$$-(\text{time-symmetric 16-pulse cycle with } X\rightarrow Y \text{ and } Y\rightarrow Z)-(16\text{-pulse cycle with } X\rightarrow Z \text{ and } Y\rightarrow X)$$
$$-(\text{time-symmetric 16-pulse cycle with } X\rightarrow Z \text{ and } Y\rightarrow X)]_n-(\pi/2)_X-(\pi/2)_Z. \tag{25}$$

A time-reversal experiment on the zero-field dipolar couplings of protons in a polycrystalline sample of adamantane was performed with sequence (25), simplified by using $k'=0$ and $k\approx 0.5$ as in sequence (23). An echo was generated after a free induction decay, as shown in Fig. 8. The observed scaling factor was close to the theoretical value of $-1/5$. A secondary echo was also obtained by further application of the sequence followed by a free evolution. Compared to sequence (25) with ideal values of k and k', the larger residual imbalance of the 16-pulse subcycles in the experiment was not found to give any noticeable effects, due to the presence of many other error sources. The damping of the echo amplitude comes from five main imperfections: nonideal pulse profiles, imbalances between pulse edges in the three coils, eddy currents, insufficient time delays between pulses, and higher-order terms in the average Hamiltonian. The actual pulses in the spectrometer deviated from the ideal ''square'' shapes assumed in the compensation schemes presented so far. Furthermore, although the inductances of the three X, Y, and Z coils were similar, their volumes and efficiencies dif-

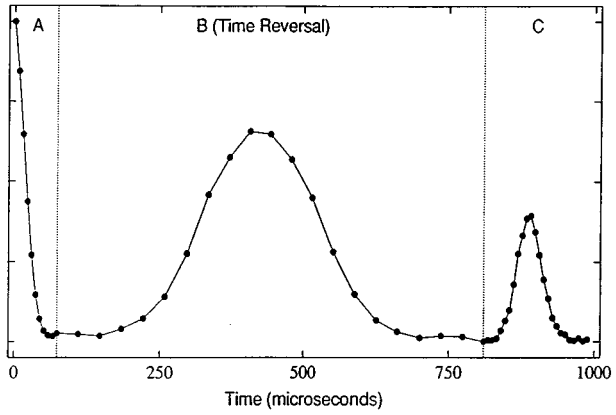

FIG. 8. Isotropic spin echoes for zero-field second-rank interactions: (A) The magnetization of the protons in polycrystalline adamantane decays due to the local isotropic dipole–dipole couplings; (B) After 74 μs, the isotropic time-reversal sequence (7) is applied and the magnetization is retrieved 380 μs later for an observed scaling factor of 19.5%, which is close to the expected theoretical scaling factor of 20.1%≈1/5; (C) Free evolution in the zero field is resumed at time 802 μs, resulting in a second echo at 880 μs. The 96-pulse sequence (25) was compensated for second-order effects and finite pulse lengths (see Sec. V). The signal was sampled at every 16-pulse subcycle of 36.4 μs, and the π/2-pulse duration was 1 μs.

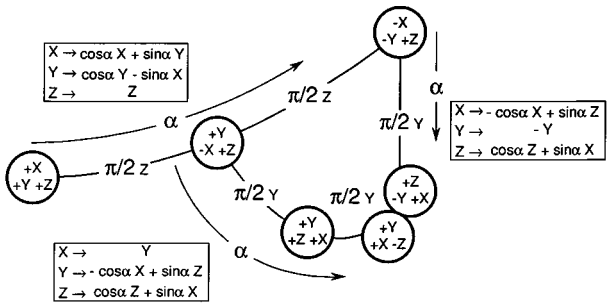

FIG. 9. Schematic representation of configurations of the five cubic classes connected by π/2 pulses. The transformations of the three Cartesian tensors X, Y, and Z are shown for the configurations along the paths designated by the pulse angle α.

fered by up to a factor of three, so the corresponding rising and falling edges were different for various pulses and the global cubic symmetry of the pulses was not strictly observed. These two effects are certainly not negligible, since in our spectrometer the duration of each π/2 pulse was $\tau=1$ μs, while the rising and falling times where estimated in part I[16] to be of similar duration (using measured pulse profiles, lower-symmetries schemes might be designed to compensate for these effects). Furthermore, the time interval between the pulses $\tau=0.9$ μs was barely longer than the pulse transients and some interference between successive pulses could thus be expected. Finally, higher-order terms in the average Hamiltonian were non negligible, since the 16-pulse subcycle duration (36.4 μs) was comparable to the typical period of the local interactions in adamantane (where the free induction decay in a zero field lasts about 50 μs).

Despite all those error sources however, the cubic sequences are more efficient than the icosahedral sequences previously described.[16] The total power requirements of the pulse-length compensated schemes are similar, they do not induce any ''orientation-transient'' errors (due to the different behavior of the coils when generating pulses of random axes), and they are much simpler to calibrate. For example, the optimal icosahedral time-reversal scheme of second-rank interactions at $\cos\omega=-1/4$ involves 12 pulses per sampling cycle for a total angle of about $7.2\times\pi$,[16] compared to 16 pulses and a total $8\times\pi$ angle for the equivalent cubic sequence (21), but it needs to be recycled five times, instead of three in the cubic case to achieve the compensation for the finite pulse lengths. It should be noticed that in any case these values are about an order of magnitude above the requirements for the corresponding high-field experiments; the optimal time-reversal scheme of second-rank interactions (which can be derived from WHH[2]) involves only two pulses per cycle with a total angle of π and is recycled twice for pulse compensation.

VI. CONCLUSION

We have shown the feasibility of practical pulse-irradiation schemes to isotropically scale the various spin couplings in zero-field NMR. Group-theoretical considerations make it possible to generate such sequences using only π/2 pulses along the three orthogonal coordinate axes. This approach provides also error compensation methods (second-order averaging terms, finite pulse lengths, eddy currents generation, etc.). Although theoretically less efficient than the optimal icosahedral sequences reported in the first part of this work,[16] these cubic sequences yield, within 20%, all of the theoretically allowed scaling factors with considerably easier experimental constraints.

Two experimental examples of cubic-symmetric sequences were shown for time reversal of first- and second-rank interactions. As already said in the first part of this work,[16] time-reversal opens new interesting opportunities allowing, for example, a zero-field analog of the high-field multiple-quantum NMR technique. This method, which we shall call ''multipolar zero-field NMR,'' yields simpler spectra for many-spin systems by reducing the number of transitions, while preserving the isotropy of spectra, in contrast with multiple-quantum HF-NMR. This could provide a new tool for structural investigations of solid-state samples, even if they are polycrystalline or amorphous.

APPENDIX A: CALCULATION OF THE ISOTROPY IMBALANCE FOR π/2 PULSES OF FINITE LENGTH

As explained in Sec. III, the average over the cubic group of a transformation of second-rank tensors can be obtained by computing the partial traces over the $\alpha\alpha$ and $\alpha\beta$ sets of second-rank Cartesian tensors. We shall thus compute this trace over some chosen simple paths, as in Fig. 9. The transformations of first-rank Cartesian tensors are the same as those of usual three dimensional vectors as given in Fig. 9. Along the $0\rightarrow\pi$ path, the second-rank tensors transform according to

$$
\begin{aligned}
&XX-YY\rightarrow(cX+sY)^2-(cY-sX)^2=c^2(XX-YY)+s^2(-XX+YY)+\cdots= && (c^2-s^2)(XX-YY)+\cdots\\
&ZZ\rightarrow && ZZ\\
&YZ\rightarrow(cY-sX)Z= && cYZ+\cdots\\
&ZX\rightarrow Z(cX+sY)= && cZX+\cdots\\
&XY\rightarrow(cX+sY)(cY-sX)= && (c^2-s^2)XY+\cdots\ ,
\end{aligned}
\tag{A1}
$$

where $c=\cos\alpha$, $s=\sin\alpha$. We used the $(XX-YY,ZZ)$ basis for the E representation (with $XX+YY+ZZ=0$). Only the diagonal terms are retained in Eq. (A1), since all others are irrelevant to calculate the traces. It is thus found

$$k_{\alpha\alpha}=c^2, \tag{A2a}$$

$$k_{\alpha\beta}=(2c^2+2c-1)/3. \tag{A2b}$$

The isotropic scaling is related to ω by Eq. (4b), and for this path $\alpha=\omega$. This allows us to calculate δ and after some elementary transformations the expressions of the first line in Table III are found.

In a similar way, along the $\pi/2\rightarrow\pi'$ path, the second-rank tensors transform according to

$$
\begin{aligned}
&XX-YY\rightarrow YY-(-cX+sZ)^2=YY-c^2XX+\cdots= && -(1+c^2)(XX-YY)/2+\cdots\\
&ZZ\rightarrow(cZ+sX)^2=c^2ZZ+s^2XX+\cdots= && (c^2-s^2/2)ZZ+\cdots\\
&YZ\rightarrow(-cX+sZ)(cZ+sX)= && 0+\cdots\\
&ZX\rightarrow(cZ+sX)Y= && 0+\cdots\\
&XY\rightarrow Y(-cX+sZ)= && -cXY+\cdots\ ,
\end{aligned}
\tag{A3}
$$

which yields

$$k_{\alpha\alpha}=(c^2-1)/2, \tag{A4a}$$

$$k_{\alpha\beta}=-c/3. \tag{A4b}$$

The isotropic scaling of a configuration at α can be obtained by calculating the relationship between α and ω, or by using the total trace of Eq. (A3). Instead of applying the general formula for the composition of rotations, we can easily derive an expression for ω as a function of α by using the first-rank isotropic scaling. It is obtained from the trace on the first-rank basis and along the $\pi\rightarrow\pi'$ path we get

$$2\cos\omega+1=\cos\alpha. \tag{A5}$$

Hence the formulas in the second line of Table III. The last and simplest line is calculated in a similar way.

The δ vs ω curves shown in Fig. 3 are obtained by eliminating α in the expressions of Table III. It is found for the two $0\rightarrow\pi$ and $\pi/2\rightarrow\pi'$ paths

$$\delta=(\cos\omega-1)^2/5, \tag{A6a}$$

$$\delta=(6\cos^2\omega+8\cos\omega+1)/5, \tag{A6b}$$

This last expression has a zero at $\cos\omega=c_0=(\sqrt{10}-4)/6\approx-0.14$. It is remarkable that we have $k_1=-k_2=(\sqrt{10}-1)/9\approx0.24$ for this point.

APPENDIX B: ALLOWED SCALING-FACTOR COMBINATIONS FOR $\pi/2$ PULSES OF FINITE LENGTH

For $\cos\omega$ above $c_0=(\sqrt{10}-4)/6$, all the $\pi/2$ paths of the cubic group display a positive isotropy imbalance δ, as shown in Fig. 3. To obtain isotropic trajectories containing configurations in this range, it is necessary to combine them with configurations at $\cos\omega$ below c_0. The range of allowed scaling factors will be given by the convex envelope of the isotropic combinations involving only two values of $\cos\omega$.

There are two such regimes of compensations, depending on whether the configuration at $\cos\omega>c_0$ is on the $0\rightarrow\pi$ or the $\pi/2\rightarrow\pi'$ paths. We shall denote the values of $\cos\omega$ in the sequence by c_1 and c_2, with weights λ and $1-\lambda$. According to Eqs. (A6), the isotropic conditions are

$$\lambda(c_1-1)^2/5+(1-\lambda)(6c_2^2+8c_2+1)/5=0, \tag{B1a}$$

$$\lambda(6c_1^2+8c_1+1)/5+(1-\lambda)(6c_2^2+8c_2+1)/5=0, \tag{B1b}$$

depending on whether the c_1 point belongs to the $0\rightarrow\pi$ or the $\pi/2\rightarrow\pi'$ paths. The scaling factors are given by

$$k_1=\lambda(2c_1+1)/3+(1-\lambda)(2c_2+1)/3, \tag{B2a}$$

$$k_2=\lambda(4c_1^2+2c_1-1)/5+(1-\lambda)(4c_2^2+2c_2-1)/5. \tag{B2b}$$

For each value of c_1 there will be a continuous set of combined λ and c_2 values that can give isotropic schemes. This defines a curve of associated (k_1,k_2) combinations. The accessible scaling factors will now be limited by the envelope of all these curves for varying c_1. This family of curves can

be parametrized in various ways and we shall perform a trigonometrical change of the variables c_1, c_2, and λ to simplify further calculations.

First we examine the case of compensation by configurations belonging to the $\pi/2 \rightarrow \pi'$ paths, as defined in Eq. (B1b). Multiplying Eq. (B1b) by 2/3 and subtracting from Eq. (B2b), we simplify the second-rank scaling factor to the following form:

$$k_2 = -\lambda(2c_1+1)/3 - (1-\lambda)(2c_2+1)/3 = -k_1. \quad \text{(B3)}$$

This result holds whenever anisotropies are compensated between two configurations belonging to the $\pi/2 \rightarrow \pi'$ path. Indeed, this was already observed for the isotropic combinations of the $\pi/2$ configuration with either $2\pi/3$ or π', as listed in Table II, and also for the configuration at $\omega = \omega_0$, as shown in Appendix A. The envelope of the scaling-factor curves in this case is trivially given by $k_2 = -k_1$.

The case of compensation by configurations belonging to the $0 \rightarrow \pi$ paths, as defined in Eq. (B1a), is less trivial. To take advantage of the fact that $0 \leqslant \lambda \leqslant 1$ and that c_1 and c_2 behave symmetrically in Eqs. (B2), we introduce the three parameters α, r, and β such that

$$\cos\,\alpha = \lambda^{1/2}, \quad \text{(B4a)}$$

$$r\,\cos\,\beta = c_1\,\cos\,\alpha, \quad \text{(B4b)}$$

$$r\,\sin\,\beta = c_2\,\sin\,\alpha, \quad \text{(B4c)}$$

In this way we preserve the symmetry between c_1 and c_2 and obtain the simple relationships: $\lambda = \cos^2\alpha$, $1-\lambda = \sin^2\alpha$, $\lambda c_1^2 + (1-\lambda)c_2^2 = r^2$, $\lambda c_1 + (1-\lambda)c_2 = r\cos(\alpha-\beta)$, $\lambda c_1^2 - (1-\lambda)c_2^2 = r^2\cos(2\beta)$, and $\lambda c_1 - (1-\lambda)c_2 = r\cos(\alpha+\beta)$. Equations (B2) and Eq. (B1a) can be rewritten as

$$k_1 = (2r\,\cos(\alpha-\beta)+1)/3, \quad \text{(B5a)}$$

$$k_2 = (4r^2 + 2r\,\cos(\alpha-\beta)-1)/5, \quad \text{(B5b)}$$

$$(7/2)r^2 - (5/2)r^2\,\cos(2\beta) + 3r\,\cos(\alpha-\beta) - 5r\,\cos(\alpha+\beta) + 1 = 0. \quad \text{(B5c)}$$

In contrast to Eqs. (B2), the scaling factors are now given as functions of just two independent parameters, r and α–β, whereas the constraint (B5c) involves β as well. By eliminating r and α–β, an implicit relationship between k_1, k_2, and β can be found, and its partial derivative with respect to β must vanish along the envelope curve. The derivative of Eq. (B5c) with respect to β, keeping r and α–β constant, yields a supplementary condition

$$r\,\sin(2\beta) + 2\,\sin(\alpha+\beta) = 0. \quad \text{(B6)}$$

An implicit relationship between k_1 and k_2 on the envelope curve can thus be obtained by eliminating r, α–β, and β, between Eqs. (B5) and (B6). After some lengthy but straightforward algebra it is found that

$$3k_2^2 - 6k_1k_2 + 9k_1^2 - 4k_2 - 2 = 0. \quad \text{(B7)}$$

This equation defines an ellipse in the (k_1, k_2) plane that, as expected, contains the points (1,1) and $((\sqrt{10}-1)/9, -(\sqrt{10}-1)/9)$ (the latter is the scaling combination obtained for the cubic configurations at ω_0, as shown in Appendix A). The limit found in Eq. (B3) is obviously inside the concave area limited by Eq. (B7). Thus the area of allowed scaling factors, as shown in Fig. 4, is limited by Eq. (B7) above $k_1 = (\sqrt{10}-1)/9$, and by the general boundary as given by Eqs. (4) below that k_1. The intercept with the $k_2 = 0$ axis is found at $k_1 = \sqrt{2}/3 \approx 0.47$, which is about 13% below the maximum theoretical value of $(\sqrt{5}+1)/6 \approx 0.54$. In canonical form, Eq. (B7) reads

$$(x/a)^2 + (y/b)^2 = 1, \quad \text{(B8)}$$

where:

$$\begin{pmatrix} x \\ y \end{pmatrix} = \begin{pmatrix} C & -S \\ S & C \end{pmatrix} \cdot \begin{pmatrix} k_1 \\ k_2 \end{pmatrix} + \frac{4}{3}\begin{pmatrix} S^3 \\ -C^3 \end{pmatrix}, \quad \text{(B9a)}$$

$$a = 2(2/3)^{1/2}S, \quad b = 2(2/3)^{1/2}C, \quad \text{(B9b)}$$

$$C = \frac{\sqrt{2+\sqrt{2}}}{2}, \quad S = \frac{\sqrt{2-\sqrt{2}}}{2}. \quad \text{(B9c)}$$

APPENDIX C: ISOTROPY IMBALANCE OF A D_4-SYMMETRIC SEQUENCE FOR TIME REVERSAL OF SECOND-RANK COUPLINGS

We shall analyze the anisotropy properties of the first-order average of a second-rank interaction over the path of $\pi/2$ pulses with D_4 symmetry defined by sequence (21). The analysis will be similar to that for the cubic group given in Sec. III. The pulses are assumed to be of finite length and rectangular shape.

The five second-rank Cartesian tensors now span four different irreducible representations of D_4,[19] designated as A_1, B_1, B_2, and E, for ZZ, $XX-YY$, XY, and $\{YZ,ZX\}$, respectively, (E is two-dimensional). After the D_4 symmetrization of a given configuration, the associated averaged transformation matrix scales each tensor representation. Thus there are four scaling factors which may be different. This holds because, just as in the case of the cubic symmetry explored in Sec. III, the Cartesian tensors are decomposed into nonidentical irreducible representations. To calculate the representation scaling factors, we shall use a procedure similar to that in Appendix A [Eq. (A3)], where a configuration along a $\pi/2$ path is designated by the angle α from the initial $\pi/2$ configuration (see Fig. 9).

Starting from the $\pi/2_Z$ configuration, a rotation by α along Y yields the transformation given in Eq. (A3) from which the four scaling factors can be deduced

$$k_{ZZ} = (3c^2-1)/2, \quad \text{(C1a)}$$

$$k_{XX-YY} = -(c^2+1)/2, \quad \text{(C1b)}$$

$$k_{XY} = -c, \quad \text{(C1c)}$$

$$k_{YZ,ZX} = 0, \quad \text{(C1d)}$$

where $c = \cos\alpha$. For $c = 1$ we obtain the scalings for the $\pi/2_{\pm Z}$ configurations, while the average over $\alpha = 0$ to $\pi/2$ yields the pulse scalings. For isotropic sequences we shall try to reduce the differences between the scaling factors, and therefore we introduce the four (nonindependent) imbalance factors $\delta_i = k_i - k_2$

TABLE VI. Scaling factor imbalances of various second-rank cartesian tensors (classified according to the irreducible representations of the D_4 group) corresponding to the full pulse path and different types of $\pi/2$ configurations in Fig. 7 (see Appendix C). Inspection of the signs of the k_i factors clearly shows the higher efficiency of pulse-length compensations by $\pi/2_{\pm X,\pm Y}$ configurations alone.

Configuration	δ_{ZZ}	δ_{XX-YY}	δ_{XY}	δ_{YZ},δ_{ZX}
$\pi/2$ Pulses	$(-\pi+16)/(40\pi)$	$-(11\pi+16)/(40\pi)$	$-(-\pi+6)/(10\pi)$	$(\pi-1)/(10\pi)$
$\pi/2_{\pm Z}$	6/5	−4/5	−4/5	1/5
$\pi/2_{\pm X,\pm Y}$	−3/10	7/10	1/5	−3/10

$$\delta_{ZZ}=(13c^2+2c-3)/10, \tag{C2a}$$

$$\delta_{XX-YY}=-(7c^2-2c+3)/10, \tag{C2b}$$

$$\delta_{XY}=-(c^2+4c-1)/5, \tag{C2c}$$

$$\delta_{YZ,ZX}=-(c^2-c-1)/5, \tag{C2d}$$

obtained from Eqs. (C1) using the isotropic scaling factor listed in Table III.

Similarly, starting with a $\pi/2_X$ configuration for instance, we shall get the scaling factors for the configurations on the vertical faces of the trajectory (see Fig. 7). The corresponding transformation can be deduced from Eq. (A3) by circularly permuting X, Y, and Z (which is a $2\pi/3$ rotation along $\langle 111\rangle$). It is then found that

$$\delta_{ZZ}=-(2c^2-2c+3)/10, \tag{C3a}$$

$$\delta_{XX-YY}=(8c^2+2c-3)/10, \tag{C3b}$$

$$\delta_{XY}=-(c^2-c-1)/5, \tag{C3c}$$

$$\delta_{YZ,ZX}=-(2c^2+3c-2)/10, \tag{C3d}$$

where the scalings at $\pi/2_{\pm X,\pm Y}$ are obtained for $c=1$, while for the pulses the average over α is needed.

Now we are interested in analyzing the isotropy imbalance of the 16-pulse cycle (21) where all the pulses are supposed to be of the same duration, whether they connect the $\pi/2_{\pm Z}$ or $\pi/2_{\pm X,\pm Y}$ configurations. We shall thus average the scaling imbalances obtained from Eqs. (C2) and (C3) over the whole group of sixteen pulses. The results are listed in Table VI with the imbalances of the two types of $\pi/2$ configurations. Ideally, the differences between the four scaling factors of the pulses should be canceled by combinations with the $\pi/2_{\pm Z}$ and $\pi/2_{\pm X,\pm Y}$ configurations. However, this cannot be done rigorously, since we are faced with three equations with two parameters only. It must be noticed that in this compensation the $2\pi/3$ configurations cannot be used not only because their scaling factors are linear combinations of those of $\pi/2_{\pm Z}$ and $\pi/2_{\pm X,\pm Y}$ (we know a linear combination of these configurations to be isotropic, see Table II), but also because the cubic symmetric analysis in Sec. III shows that the pulse paths have to be combined with $\pi/2$ configurations only (see Table V).

The analysis of cubic-symmetric pulse compensation in Sec. III gave the relative weights between the $\pi/2\rightarrow 2\pi/3$ pulses and $\pi/2$ configurations (see Table V). We shall thus introduce the same global weighing factors in our present D_4-symmetric analysis, but the relative weights of the $\pi/2_{\pm Z}$ and $\pi/2_{\pm X,\pm Y}$ configurations may now depart from the cubic-symmetric values. If λ and $1-\lambda$ represent these weights and if bold $\boldsymbol{\delta}$'s are used for the four-dimensional vectors of scaling imbalances (whose components are given in Table VI), the global imbalance of a compensation scheme can be written as

$$\boldsymbol{\delta}_{\text{Scheme}}(\lambda)=(4\pi)/(7\pi-8)\,\boldsymbol{\delta}_{\text{Pulses}}+(3\pi-8)/(7\pi-8)\times[\lambda\,\boldsymbol{\delta}_{\pm X,\pm Y}+(1-\lambda)\,\boldsymbol{\delta}_{\pm Z}], \tag{C4}$$

using the global weights given in Table V. Although there is no λ which could cancel $\boldsymbol{\delta}_{\text{Scheme}}$ and give an isotropic behavior, it is still possible to minimize its magnitude. In this way the mean anisotropic part of the averaged second-rank tensors will reach a minimum. The mean square imbalance over the five-dimensional space of second-rank tensors will be given by

$$\|\boldsymbol{\delta}\|^2=(\delta_{ZZ}^2+\delta_{XX-YY}^2+\delta_{XY}^2+2\,\delta_{YZ,ZX}^2)/5, \tag{C5}$$

where the factor 2 accounts for the fact that the E representation is two-dimensional. Inserting Eq. (C4) into Eq. (C5) with the scaling factors from Table V, after some elementary algebra one finds

$$5(7\pi-8)^2\|\boldsymbol{\delta}_{\text{Scheme}}(\lambda)\|^2=(61\pi^2-272\pi+304)-(81\pi^2-396\pi+480)\lambda+(54\pi^2-288\pi+384)\lambda^2. \tag{C6}$$

The minimization of this expression as a function of λ gives the optimum weight

$$\lambda_{\text{Opt}}=(9\pi-20)/(12\pi-32)\approx 1.452, \tag{C7}$$

which is greater than one. Thus $\lambda=1$ is the closest to the optimum and incidentally it corresponds to the sequence (23). The average anisotropic contribution during the compensated pulses can then be found as

$$\|\boldsymbol{\delta}_{\text{Scheme}}(1)\|=(\sqrt{7}/\sqrt{10})(4-\pi)/(7\pi-8)\approx 5.13\%. \tag{C8}$$

This value is not negligible when compared to the isotropic scaling of −20%, but it is still much smaller than that obtained at $\lambda=2/3$ when all the $\pi/2$ configurations are evenly weighed

$$\|\boldsymbol{\delta}_{\text{Scheme}}(2/3)\|=(1/\sqrt{30})(3\pi^2+16)^{1/2}/(7\pi-8)\approx 8.81\%. \tag{C9}$$

Although Eq. (C7) yields an apparently unrealistic negative weight for the $\pi/2_{\pm Z}$ configurations, this result can still be used. By further adding the standard cubic-symmetric

combination of $\pi/2$ and $2\pi/3$ configurations (as given in Table II), it is possible to cancel the weight of the negative $\pi/2_{\pm Z}$ configurations. In this way the most efficient compensation scheme can be generated. The corresponding weights for this scheme are found as

$$\lambda_{\text{Pulses}}=16\pi/(13\pi+28)\approx 0.730, \tag{C10a}$$

$$\lambda_{\pi/2,\pm X\pm Y}=(3\pi+4)/(13\pi+28)\approx 0.195, \tag{C10b}$$

$$\lambda_{2\pi/3}=(-6\pi+24)/(13\pi+28)\approx 0.075, \tag{C10c}$$

which yields the mean square imbalance

$$\|\delta_{\text{Scheme}}(\lambda_{\text{Opt}})\|=(1/\sqrt{10})(4-\pi)/(14\pi-16)\approx 0.97\%. \tag{C11}$$

This result is at least a factor of 5 better than the crude compensations examined before [see Eqs. (C8) and (C9)]. When compared with the individual length of the pulses the weighing coefficients in Eqs. (C10) become

$$\lambda_{\text{Pulses}}=16, \tag{C12a}$$

$$\lambda_{\pi/2,\pm X\pm Y}=3+4/\pi\approx 4.27, \tag{C12b}$$

$$\lambda_{2\pi/3}=-6+24/\pi\approx 1.64, \tag{C12c}$$

from which sequence (24) is deduced.

ACKNOWLEDGMENTS

We are grateful to J. Sachleben for his help with the experiments. This work was supported by the Director, Office of Energy Research, Office of Basic Energy Sciences, Materials Sciences Division of the U.S. Department of Energy under Contract No. DE-AC03-76SF00098. A.L. also acknowledges financial support from the Commissariat á l'Energie Atomique, France, and from the North-Atlantic Treaty Organization (Grant No. 68C89FR).

[1] A. Abragam, *Principles of Nuclear Magnetism* (Clarendon, Oxford, 1961); C. P. Slichter, *Principles of Magnetic Resonance*, 3rd ed. (Springer, Berlin, 1990).
[2] M. Mehring, *Principles of High Resolution NMR in Solids* (Springer-Verlag, Berlin, 1983); U. Haeberlen, *Advances in Magnetic Resonance Suppl. 1* (Academic, New York, 1976), 2nd ed.
[3] R. R. Ernst, G. Bodenhausen, and A. Wokaun, *Principles of NMR in One and Two Dimensions* (Oxford Scientific, Oxford, 1987); C. A. Fyfe, *Solid State NMR for Chemists* (C.F.C., Guelph, 1983).
[4] E. R. Andrew, A. Bradbury, and R. G. Eades, Nature (London) **182**, 1659 (1958); I. J. Lowe, Phys. Rev. Lett. **2**, 285 (1959).
[5] J. S. Waugh, L. M. Huber, and U. Haeberlen, Phys. Rev. Lett. **20**, 180 (1968); U. Haeberlen and J. S. Waugh, Phys. Rev. **175**, 453 (1968).
[6] A. Llor and J. Virlet, Chem. Phys. Lett. **152**, 248 (1988); B. F. Chmelka, K. T. Mueller, A. Pines, J. Stebbins, Y. Wu, and J. W. Zwanziger, Nature (London) **339**, 42 (1989).
[7] A. Samoson, E. Lippmaa, and A. Pines, Mol. Phys. **65**, 1013 (1988).
[8] D. P. Weitekamp, A. Bielecki, D. Zax, K. Zilm, and A. Pines, Phys. Rev. Lett. **50**, 1807 (1983); D. Zax, A. Bielecki, K. Zilm, A. Pines, and D. P. Weitekamp, J. Chem. Phys. **83**, 4877 (1985).
[9] E. L. Hahn, Phys. Rev. **80**, 580 (1950).
[10] H. Schneider and H. Schmiedel, Phys. Lett. A **30**, 298 (1969).
[11] W.-K. Rhim, A. Pines, and J. S. Waugh, Phys. Rev. Lett. **25**, 218 (1970); W.-K. Rhim, A. Pines, and J. S. Waugh, Phys. Rev. B **3**, 684 (1971); K. Takegoshi and C. A. McDowell, Chem. Phys. Lett. **116**, 100 (1985).
[12] D. P. Weitekamp, Adv. Magn. Reson. **11**, 111 (1983); M. Munowitz and A. Pines, Adv. Chem. Phys. **LXVI**, 1 (1987).
[13] C. J. Lee, D. Suter, and A. Pines, J. Mag. Res. **75**, 110 (1987).
[14] A. Llor, D.Sc. thesis (in French), Université Paris XI, Orsay, 1987.
[15] A. Llor, Z. Olejniczak, J. Sachleben, and A. Pines, Phys. Rev. Lett. **67**, 1989 (1991).
[16] A. Llor, Z. Olejniczak, and A. Pines, J. Chem. Phys. **103**, 3966 (1995).
[17] A. Llor and Z. Olejniczak (unpublished).
[18] A. Bielecki, D. Zax, K. Zilm, and A. Pines, Rev. Sci. Instrum. **57**, 393 (1986).
[19] E. P. Wigner, *Group Theory and its Applications to the Quantum Mechanics of Atomic Spectra* (Academic, New York, 1959); M. Hamermesh, *Group Theory and its Applications to Physical Problems* (Dover, New York, 1989); J.-Q. Chen, *Group Representation Theory for Physicists* (World Scientific, Singapore, 1989).
[20] S. L. Sobolev, Dokl. Akad. Nauk SSSR **146**, 310 (1962); S. L. Sobolev, Dokl. Akad. Nauk SSSR **146**, 770 (1962).
[21] A. H. Stroud, *Approximate Calculation of Multiple Integrals* (Prentice-Hall, Englewood Cliffs, NJ, 1971); A. M. Tam, Ph.D. dissertation, University of California, Berkeley, 1982.